

Geophysical Research Letters

RESEARCH LETTER

10.1029/2020GL090707

Special Section:

Fire in the Earth System

Key Points:

- Geostationary satellite observations of fire radiative power are highly correlated with in situ airborne measurements of primary-emission smoke tracers
- High-resolution satellite observations are needed to disentangle how fire activity and plume dilution impact the downwind evolution of smoke
- Diurnal fire activity for wildfires observed during FIREX-AQ is best parameterized using a bimodal Gaussian distribution to inform models

Supporting Information:

- Supporting Information S1

Correspondence to:

E. B. Wiggins and R. H. Moore,
 elizabeth.b.wiggins@nasa.gov;
 richard.h.moore@nasa.gov

Citation:

Wiggins, E. B., Soja, A. J., Gargulinski, E., Halliday, H. S., Pierce, R. B., Schmidt, C. C., et al. (2020). High temporal resolution satellite observations of fire radiative power reveal link between fire behavior and aerosol and gas emissions. *Geophysical Research Letters*, 47, e2020GL090707. <https://doi.org/10.1029/2020GL090707>

Received 10 SEP 2020


















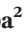

Accepted 9 NOV 2020

Accepted article online 23 NOV 2020

©2020. The Authors.

This is an open access article under the terms of the Creative Commons Attribution License, which permits use, distribution and reproduction in any medium, provided the original work is properly cited.

High Temporal Resolution Satellite Observations of Fire Radiative Power Reveal Link Between Fire Behavior and Aerosol and Gas Emissions

Elizabeth B. Wiggins^{1,2} , Amber J. Soja^{2,3} , Emily Gargulinski³ , Hannah S. Halliday⁴ , R. Bradley Pierce⁵ , Christopher C. Schmidt⁵, John B. Nowak² , Joshua P. DiGangi² , Glenn S. Diskin² , Joseph M. Katich^{6,7} , Anne E. Perring⁸ , Joshua P. Schwarz⁷ , Bruce E. Anderson² , Gao Chen², Ewan C. Crosbie^{2,9} , Carolyn Jordan^{2,3} , Claire E. Robinson^{2,9}, Kevin J. Sanchez^{1,2}, Taylor J. Shingler², Michael Shook² , Kenneth L. Thornhill^{2,9} , Edward L. Winstead^{2,9} , Luke D. Ziemba² , and Richard H. Moore² 

¹NASA Postdoctoral Program, Universities Space Research Association, Columbia, MD, USA, ²NASA Langley Research Center, Hampton, VA, USA, ³National Institute of Aerospace, Hampton, VA, USA, ⁴Environmental Protection Agency, Research Triangle, NC, USA, ⁵Space Science and Engineering Center, University of Wisconsin-Madison, Madison, WI, USA, ⁶CIRES, University of Colorado Boulder, Boulder, CO, USA, ⁷NOAA Chemical Sciences Laboratory, Boulder, CO, USA, ⁸Department of Chemistry, Colgate University, Hamilton, NY, USA, ⁹Science Systems and Applications, Inc., Hampton, VA, USA

Abstract Wildfire smoke influences on air quality and atmospheric chemistry have been underscored by the increasing fire prevalence in recent years, and yet, the connection between fire, smoke emissions, and the subsequent transformation of this smoke in the atmosphere remains poorly constrained. Toward improving these linkages, we present a new method for coupling high time-resolution satellite observations of fire radiative power with in situ observations of smoke aerosols and trace gases. We apply this technique to 13 fire plumes comprehensively characterized during the recent FIREX-AQ mission and show that changes in fire radiative power directly translate into changes in conserved smoke tracers (CO₂, CO, and black carbon aerosol) observed in the downwind smoke plume. The correlation is particularly strong for CO₂ (mean $r > 0.9$). This method is important for untangling the competing effects of changing fire behavior versus the influence of dilution and atmospheric processing on the downwind evolution of measured smoke properties.

1. Introduction

Wildfire activity in the Western United States causes poor air quality, adverse human health impacts, and substantial economic costs (Jaffe et al., 2008; Kochi et al., 2010; Liu et al., 2015; Lu et al., 2016; Reid et al., 2016; Stavros et al., 2014). The frequency and intensity of these fires are expected to increase in the future due to a combination of growing human settlement at the wildland urban interface and climate change (Abatzoglou & Williams, 2016; Hammer et al., 2009; Mell et al., 2010; Theobald & Romme, 2007; Westerling et al., 2006). Consequently, it is essential to understand the composition and magnitude of aerosol and trace gas emissions from wildland fires and prescribed fires to quantify the effects of fire emissions on air quality and climate.

Fires emit a complex and highly variable mixture of gases and aerosols that can considerably alter atmospheric composition and tropospheric chemistry over a wide range of spatial and temporal scales (Bond et al., 2013; Goldammer et al., 2008; Langmann et al., 2009; Urbanski, 2014). Environmental conditions at the location of the fire, such as local weather and fuel structure, influence the composition and magnitude of these emissions (Loehman et al., 2014; Thonicke et al., 2010). Wildfires generally have a pronounced diurnal cycle directly related to weather conditions, with activity peaking early in the afternoon and diminishing after sunset (Ichoku et al., 2008; Saide et al., 2015; Zhang & Kondragunta, 2008).

Fire emissions inventories are an essential tool for understanding the spatiotemporal distribution of fire emissions on a regional to global scale. The resolution of commonly used fire emissions inventories

diverges considerably depending on their intended use and the methodology used in their development. As a result, considerable irregularities exist among fire emissions inventories in the estimated magnitude, composition, and distribution of emissions in space and time (Larkin et al., 2014; Li et al., 2019; Liu et al., 2020; Shi et al., 2015). In general, these differences can be attributed to variations in the approach used to quantify burned area, fuel loads, combustion completeness, and emission factors (Kasischke & Penner, 2004). Quantitative comparisons between different fire emissions inventories remain scarce due to the variable transport models used in each study and the spatial/temporal averaging used for comparison to observations (Liu et al., 2020). However, a few recent studies have shown significant variability in aerosol emissions from fire emissions inventories and large discrepancies between observations and fire emissions inventory driven predictions of surface aerosol concentrations (Pan et al., 2020; Xie et al., 2020).

Most fire emissions inventories employ remote sensing observations of fire parameters such as burned area, active fire counts, and fire radiative power (FRP) from instruments onboard polar orbiting satellites, including the Moderate Resolution Imaging Spectroradiometer (Ichoku & Ellison, 2014; Kaiser et al., 2012; Pierce et al., 2007; van der Werf et al., 2017; Wiedinmyer et al., 2011) and the Visible Infrared Imaging Radiometer Suite (Ahmadov et al., 2017). Typical overpass times for the satellites hosting these instruments occur only twice daily over North America at ~ 1 a.m./p.m. or at ~ 10 a.m./p.m. local time (Li et al., 2018). Due to this limited temporal coverage of fire observations in a given location, some fire emissions inventories or models supplement the diurnal cycle of emissions using FRP observations from geostationary satellites (Andela et al., 2015; Li et al., 2019; Mota & Wooster, 2018; Mu et al., 2011; Zhang et al., 2012) or assume a Gaussian distribution of daily FRP (Kaiser et al., 2009).

Geostationary satellite instruments, such as the Geostationary Operational Environmental Satellite (GOES) Advanced Baseline Imager (ABI), observe FRP for a given fire over the course of the entire diurnal cycle and at a much finer temporal resolution than their polar-orbiting counterparts. While the temporal resolution is higher, this comes at the expense of providing only hemispheric coverage and decreased spatial resolution which increases detection biases (Li et al., 2020; Schmidt, 2019). GOES ABI imagery provides a snapshot of FRP across the continental United States every 5 min and full disk FRP every 10 min (<https://www.goes-r.gov/spacesegment/abi.html>) at a relatively coarse spatial resolution of 2 km (Schmidt, 2019) and offers the opportunity to investigate both the diurnal cycle of fire activity and short-term changes in fire behavior that could have important implications for fire emission estimates (Li, Zhang, et al., 2019; Schmidt, 2019; Zhang & Kondragunta, 2008).

There is a need to connect spatially coarse, remotely sensed fire observations that have more widespread coverage and lower time resolution with in situ point source observations that have much higher spatial and temporal resolution but much lower overall coverage to achieve a more comprehensive understanding of fire behavior and emissions. Rather than using GOES FRP observations to directly estimate emissions using a top-down approach (Freeborn et al., 2008; Ichoku et al., 2008; Wooster et al., 2003), we use 5-min resolution, near real-time GOES FRP observations to quantify the relationship between FRP and in situ measurements of fire emissions. We validate this technique using airborne observations of individual fires sampled during the recent Fire Influence on Regional to Global Environments and Air Quality (FIREX-AQ) field campaign. FIREX-AQ measured the concentrations, composition, and properties of smoke from wildfires and prescribed fires in the Continental United States during the summer of 2019 using the National Aeronautics and Space Administration (NASA) DC-8 aircraft. Here we focus on the Western U.S. portion of the campaign. The GOES FRP observations are compared to the airborne in situ measurements of relatively long-lived species emitted by fires, including CO₂, CO, and black carbon (BC) mass. This work promises significant improvements for resolving the temporal resolution of emissions in new and existing daily fire emissions inventories and smoke forecasting model frameworks.

2. Methods

2.1. GOES FRP

2.1.1. GOES Diurnal Cycle of FRP

FRP is an important quantitative indicator of fire activity and how it changes over the study period. We generate an average diurnal cycle of FRP for all the Western U.S. wildland fires in FIREX-AQ by examining each sampled fire individually using FRP observations from the GOES-16 and GOES-17 ABI L2 + Fire/hot spot

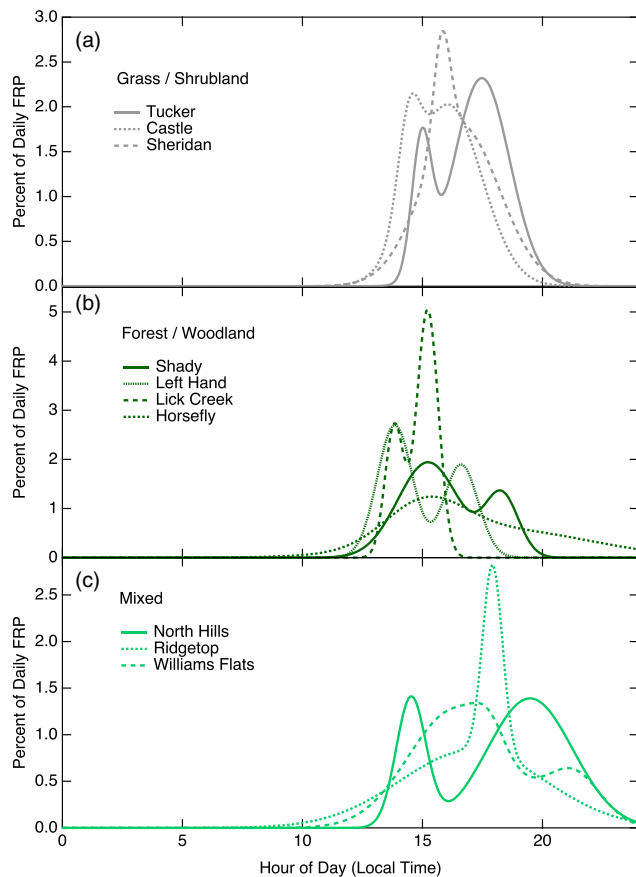


Figure 1. Bimodal Gaussian model fit of average GOES diurnal cycle (over the entire lifetime of the fire) for each fire sampled during FIREX-AQ. Classified by dominant landcover type using the final GeoMAC burned area perimeter. Model fit to FRP shown as a probability distribution over the course of a day in local time. (a) shows fires classified as grass/shrubland, (b) shows fires classified as forest/woodland, and (c) shows fires classified as mixed.

Detection and Characterization product from the Wildfire Automated Biomass Burning Algorithm processing system (Schmidt, 2019). The FRP data products for the wildland fires specific to FIREX-AQ are archived in the NASA data archive. The Wildfire Automated Biomass Burning Algorithm/Fire/hot spot Detection and Characterization product provides FRP for fires in the continental United States with a spatial resolution of 2 km and a temporal resolution of 5 min. Previous studies have found the diurnal cycle of fire activity can be modeled as a Gaussian distribution or a Fourier series (Andela et al., 2015; Giglio, 2007; Roberts et al., 2009; Zhang & Kondragunta, 2008). In this study, we choose to use a bimodal Gaussian distribution as opposed to one with a single mode, because the bimodal fit had a slightly higher correlation with the observation-driven diurnal cycle of FRP for the FIREX-AQ fires (supporting information Table S1). For each individual fire (spatially defined in the next paragraph), we derive the average diurnal cycle of FRP, defined as the fit to the total FRP (in 5-min intervals over the course of a 24-hr day in local time) averaged over every day the fire was actively burning (Figure 1). Each fire's average diurnal cycle is used to fill in observational data gaps when cloud cover or thick smoke prohibits detection. The functional form of the bimodal Gaussian distribution is

$$FRP(t) = \sum_{i=1}^2 \frac{a_i}{\sigma_i \sqrt{2\pi}} e^{-\left(\frac{t-t_i}{\sigma_i}\right)^2}, \quad (1)$$

where a_i is the FRP of mode i in units of MW, t_i is the median time of mode i in hours from midnight (local time), and σ_i is the standard deviation of mode i in hours. GOES FRP observations are included if their centroid is within 4 km of the final burned area perimeter defined by the Geospatial Multi-Agency Coordination Wildland Fire Perimeters database (Walters et al., 2011). The size of the buffer is double the diameter of the fixed grid resolution from GOES in order to capture all detections of an individual fire.

To quantify the diurnal cycle of FRP for a single fire on an individual day, any time gaps in GOES FRP observations were filled using the average Gaussian model scaled to the mean of the available FRP observations

for each fire on that day. Observational gaps often occur because of cloud cover, and on average, this occurred 34% of the time for the fires included in this analysis. The model fit is only used to interpolate missing FRP observations for days with observations of FRP > 0 spanning at least 6 hr out of the entire 24-hr (local time) period in order to avoid overestimating FRP. In practice, this data reconstruction step has negligible impact on the FRP time series for fires where data coverage is good (e.g., the Williams Flats fire highlighted in Figures 2 and S1); however, for the few fires with substantial missing observations due to cloud cover or thick smoke (e.g., Castle fire), this step is more impactful. We note fire behavior can be influenced by cloud cover, and our approach may introduce some bias when filling in gaps using a diurnal distribution built under clear or mostly clear skies.

2.1.2. Fuels and Fire Weather

To investigate the influence of fuel type on the mean diurnal cycle of FRP, we grouped fires together that shared similar fuel loading and structure according to the Fuel Characteristics and Classification System (FCCS) (Ottmar et al., 2007). The dominant ecosystem type is defined as the FCCS fuel class that encompasses at least 75% of the burned area defined by the final Geospatial Multi-Agency Coordination perimeter at the end of the fire's life cycle. It should be noted that only the dominant fuel type per fire was used for classification in this study, although each fire burned through a wide variety of fuel types, and different ratios of fuel types on different burn days are neglected. The fires included in this analysis are grouped into one of the three following fuel categories: grass/shrublands, forest/woodlands, and mixed. The mixed category is

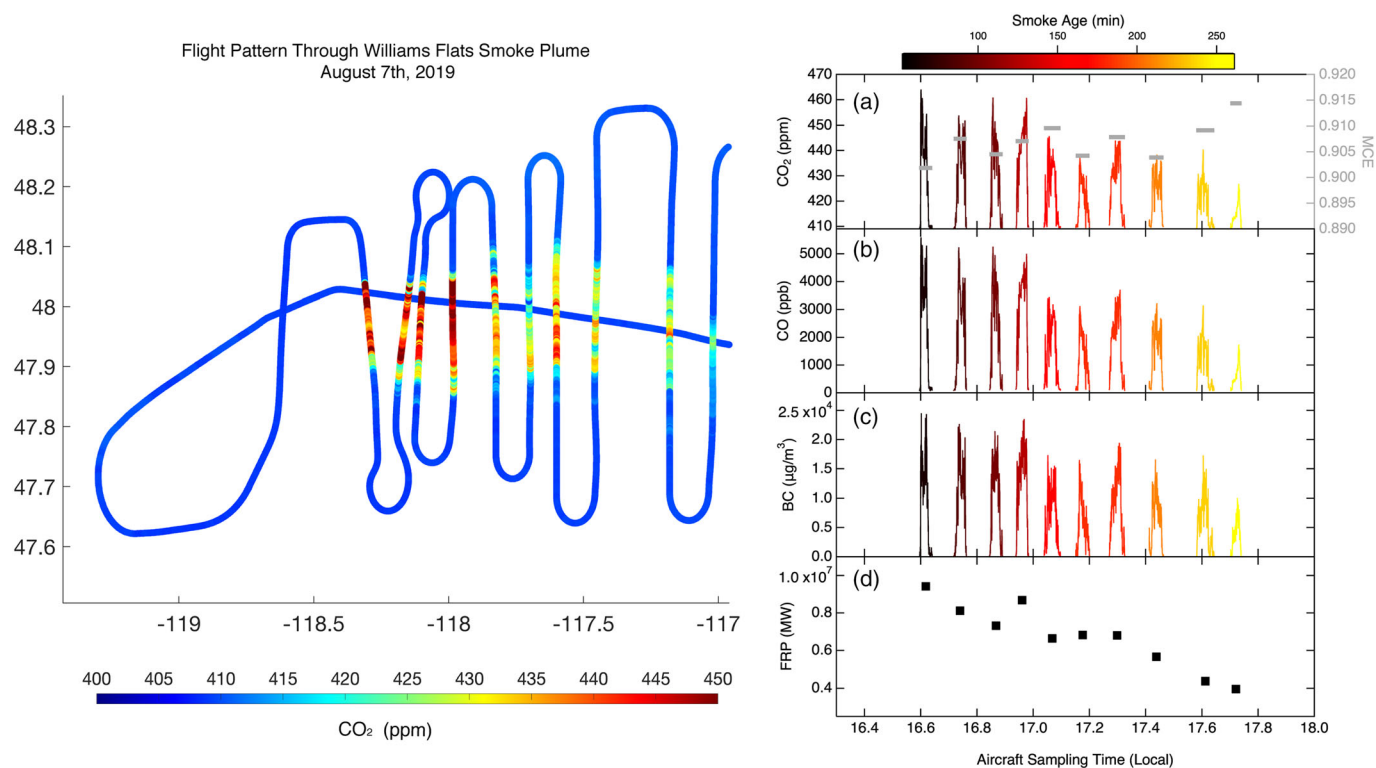


Figure 2. Left panel shows a map of the DC-8 flight track on 7 August 2019 for the first set of orthogonal transects through the Williams Flats smoke plume. Colors correspond to the CO₂ mixing ratios from DC-8 measurements. The average wind speed for the transects shown is 7.6 ± 1.6 m/s, and the average wind direction is $263 \pm 10^\circ$. Right panel shows a time series of CO₂, CO, and BC observations from the DC-8 (a–c) that correspond to the transects shown in the left panel and are highlighted by average smoke age. (d) shows GOES FRP integrated over the same time interval represented by the smoke plume transects and aligned in time with the observations.

defined as a combination of grass/shrublands and forest/woodlands for fires with less than 75% of the burned area encompassed by either grass/shrubland or forest/woodlands. Examples of specific FCCS fuel classes used in each grouping is shown in Table S2. Daily fire weather danger levels are obtained from the National Fire Danger Rating System provided by the U.S. Forest Service (Bradshaw et al., 1983).

Fires in grass/shrublands are often considered to be fuel limited, while forest fires can be considered ignition limited because of generally higher fuel moisture. The diurnal cycle of fire activity begins around the same time for all ecosystems considered (12:00 hr local time) but extended much later into the night (24:00 hr) in mixed ecosystems compared to grass/shrublands or forest/woodlands (20:00 hr), with the exception of the Horsefly fire (Figure 1). Incident reports of Horsefly indicate the fuels include a significant amount of dead and down trees caused by bark beetle damage (<https://inciweb.nwcg.gov/incident/6502/>). The longest diurnal combustion period occurs in mixed fuels and forests with high proportions of beetle killed dead and down trees. One explanation for this behavior is the finer fuels allowed for more rapid fire spread and helped to dry out the larger dead fuels. Simultaneously, smoldering combustion in coarse woody debris, including beetle killed trees, is known to continue well into the night (Albini & Reinhardt, 1995; Hyde et al., 2011). In all of the fires categorized as having mixed fuels, the invasive species cheatgrass was a component of the fuels in the burned area perimeter (24% Williams Flats, 12% North Hills, and 4% Ridgetop). Cheatgrass enhances fire size and frequency in the Western United States and can outcompete native vegetation after fire, which induces a vicious cycle where future wildfires propagate cheatgrass expansion (Balch et al., 2013; Kerns et al., 2020; Menakis et al., 2003).

2.2. Comparison With In Situ Observations

2.2.1. Aircraft Aerosol and Trace Gas Observations

We compare the high-temporal resolution GOES FRP product to the airborne measurements of CO₂, CO, and refractory BC aerosol concentrations in the FIREX-AQ smoke plumes. The DC-8 aircraft flew through each

wildfire smoke plume in a series of orthogonal plume transects starting near the fire and proceeding downwind as far as practical given mission objectives and flight limitations (Figure 2). An example set of plume transects for the Williams Flats fire in Washington State is shown in Figure 2. CO₂ mixing ratio measurements are obtained using a non-dispersive infrared (IR) spectrometer (LICOR, Inc. Model 7,000) adapted for aircraft measurements in a method similar to Vay et al. (2003), while CO mixing ratios are obtained from mid-IR laser absorption spectrometry (Sachse et al., 1991). Both species were calibrated in-flight with standards from the National Oceanic and Atmospheric Administration Earth Science Research Laboratories (NOAA ESRL) traceable to World Meteorological Organization (WMO) scales (CO₂:X2007; CO:X2014A). Refractory BC mass concentrations appropriate for most of the accumulation mode were provided by a Single Particle Soot Photometer (SP2, Droplet Measurement Technologies). CO₂ is chosen because it is the most dominant trace gas species emitted from fires (Andreae & Merlet, 2001). CO and BC are chosen for comparison because they are tracers of primarily smoldering and flaming fire processes (Sommers et al., 2014; Urbanski, 2014), respectively, and are conserved over the relatively short (hours-long) time scales of the DC-8 sampling. The modified combustion efficiency (MCE) is a metric commonly used to determine relative contributions from smoldering and flaming fire processes to emissions (Ward & Radke, 1993). MCE is calculated using the following equation:

$$MCE = \frac{1}{m_{CO/CO_2} + 1}, \quad (2)$$

where m_{CO/CO_2} is the slope of the York regression between excess mixing ratios (background subtracted) of CO and CO₂.

2.2.2. Relationships Between In Situ Measurements and GOES FRP

To compare in situ trace gas and aerosol observations with GOES FRP, we calculate the smoke age as the difference between when the smoke was emitted and when it was sampled by the DC-8, using the aircraft-measured wind speeds and assuming straight line horizontal advection between the fire and aircraft positions with uniform winds for all transects of a single plume. The average wind speed for all fires and all transects is $8 \pm 3 \text{ m s}^{-1}$, and the typical wind direction is westerly. Example wind speed and direction are given in Table S3 for the transects shown in Figures 2 and S2. The vertical transport time of the plume is neglected. We calculate the time of emission as the average time of sampling by the DC-8 aircraft across a single transect minus this smoke age.

We quantify the temporal variability of CO₂ and CO mixing ratios as well as the BC mass concentration by integrating the DC-8 measurements across each smoke plume transect following the methodology of Yokelson et al. (2007). For each orthogonal transect through the FIREX-AQ smoke plume, we integrate excess mixing ratios of CO₂, CO, and BC across the entire length of the plume cross section. Baseline concentration values used for the background subtraction are calculated as the 5-s-averaged mixing ratios of each species starting 1 s before and after each transect. We then calculate the relative rate of change of the aerosol and trace gas species and MCE for each transect, which we expect should scale proportionately with the rate of change of the FRP, after accounting for the smoke plume age, Δt , as follows:

$$\left. \frac{\partial \ln(\Delta X)}{\partial t} \right|_{t+\Delta t} \propto \left. \frac{\partial \ln(\text{FRP})}{\partial t} \right|_t, \quad (3)$$

where ΔX is the integrated excess mixing ratio of species X and t is the time corresponding to the measured FRP and estimated time of smoke emission. In this study, we compute the approximate derivative by differencing the DC-8 measurements across two adjacent aircraft transects. For each DC-8 plume transect, k (and corresponding time interval at the fire, j), the scaling relationship is calculated as

$$\frac{1}{\Delta X_k} \cdot \frac{\Delta X_k - \Delta X_{k-1}}{t_k - t_{k-1}} \propto \frac{1}{\Delta \text{FRP}_j} \cdot \frac{\Delta \text{FRP}_j - \Delta \text{FRP}_{j-1}}{t_j - t_{j-1}}, \quad (4)$$

where ΔFRP_j is the integrated FRP over the relatively short time interval represented by the aircraft sampling time minus the smoke age ($t_j = t_k - \Delta t_k$). Implicit in Equation 4 is that the smoke age can be used to extrapolate from the aircraft sampling time back to the time of emission at the fire. Furthermore,

we assume that the conserved species in the plume do not continue to evolve between adjacent transects (i.e., $\Delta t_k - \Delta t_{k-1} = 0$). While this assumption may be reasonably valid for the conserved tracers examined here whose plume evolution is mainly impacted by dilution, it is likely to break down for other extensive aerosol and trace gas variables that are strongly influenced by photochemical processing, coagulation, and gas-particle partitioning of semi-volatile compounds. Applying Equation 3 for those variables for FIREX-AQ will be more complicated, as the spacing of the DC-8 sampling transects along the plume length do not reflect a 1:1 increase in both smoke age and sampling time interval. Figure S3 demonstrates that this ratio varies from 0.8–6.4 across the FIREX-AQ wildfires. In most cases, the time it takes the aircraft to sample successive downwind portions of the plume is considerably shorter than the time it takes for the plume to be advected over the intervening distance, assuming straight-line, horizontal advection.

We compute Pearson's correlation coefficients to quantify the linear proportionality between transect-integrated values of CO₂, CO, and BC versus FRP as represented by Equation 4. While strong correlation coefficients would be hypothesized to indicate the governing influence of fire activity on emissions, weaker correlation coefficients may indicate the presence of important, confounding processes such as smoke plume dilution. The importance of dilution for driving smoke variability may also vary at specific locations within the plume (e.g., near the edges vs. the center) in ways that are not captured by this integrated plume analysis. Similarly, the nature of the aircraft horizontal sampling transects prevents us from examining changes in the vertical structure of these conserved tracer species that may be impacted by boundary layer convective mixing, dilution, or size-dependent particle gravitational settling.

3. Results and Discussion

3.1. GOES FRP Diurnal Cycles

We investigate the average diurnal cycle of FRP on the scale of individual fires in the Western United States grouped according to the dominant ecosystem represented by the burned area (Figure 1 and Table S1). The diurnal cycle of FRP for all fires in this analysis is optimally fit using a bimodal Gaussian distribution. Coefficients of the bimodal Gaussian distribution for all fires are tabulated in Table S1. Pearson's correlation coefficients (r) between single-mode Gaussian distributions and bimodal Gaussian distributions (Table S1) demonstrate the ability to model diurnal fire activity and highlight the slight differences between single and bimodal distributions.

Our results suggest a bimodal Gaussian distribution could improve the accuracy of the timing of fire emissions in fire emissions inventories and smoke forecasting models. The fires tend to peak later in the day than might be expected based on past literature (Giglio, 2007; Pack et al., 2000; Roberts et al., 2009; Zhang & Kondragunta, 2008), but the model standard deviations of 1–2 hr are consistent with common model assumptions.

The bimodal Gaussian distribution has been observed in other ecosystems (Giglio, 2007; Pack et al., 2000). It is unclear whether the trough between the peaks is a true measure of reduced fire activity or a result of detection bias. The contrast between fire pixels and surrounding non-fire pixels is reduced around solar noon, and the bimodal model fit could be an artifact of detection bias (Giglio et al., 1999). Alternatively, fire detection could be inhibited by thick cloud or smoke cover. In the presence of clouds, higher atmospheric moisture would act to reduce fire activity and supports our bimodal model fit. The short-term variability in fire activity is known to be strongly influenced by weather conditions and synoptic-scale meteorological events (Schroeder, 1970; Wiggins et al., 2016), and it is possible the bimodal model fit represents the fast response to changing environmental conditions. We note the bimodal model fit is specific to fires in the Western United States and advise against its application on a global scale across ecosystems with much different fire regimes.

We find the timing and magnitude of peaks in the bimodal Gaussian fit of the diurnal distribution of FRP vary between all fires, but there are discernible differences between the ecosystems represented by the fires analyzed. Overall, the 5-min data reveal significant time-varying structure in fire activity, which needs to be accounted for when examining the fire plume characteristics across different aging time scales.

3.2. Relationships Between Integrated GOES FRP and In Situ Measurements

Our approach allows for direct comparison of satellite FRP observations with 1 Hz aircraft trace gas and aerosol observations at an extremely high time resolution of 5-min intervals. The strong linear

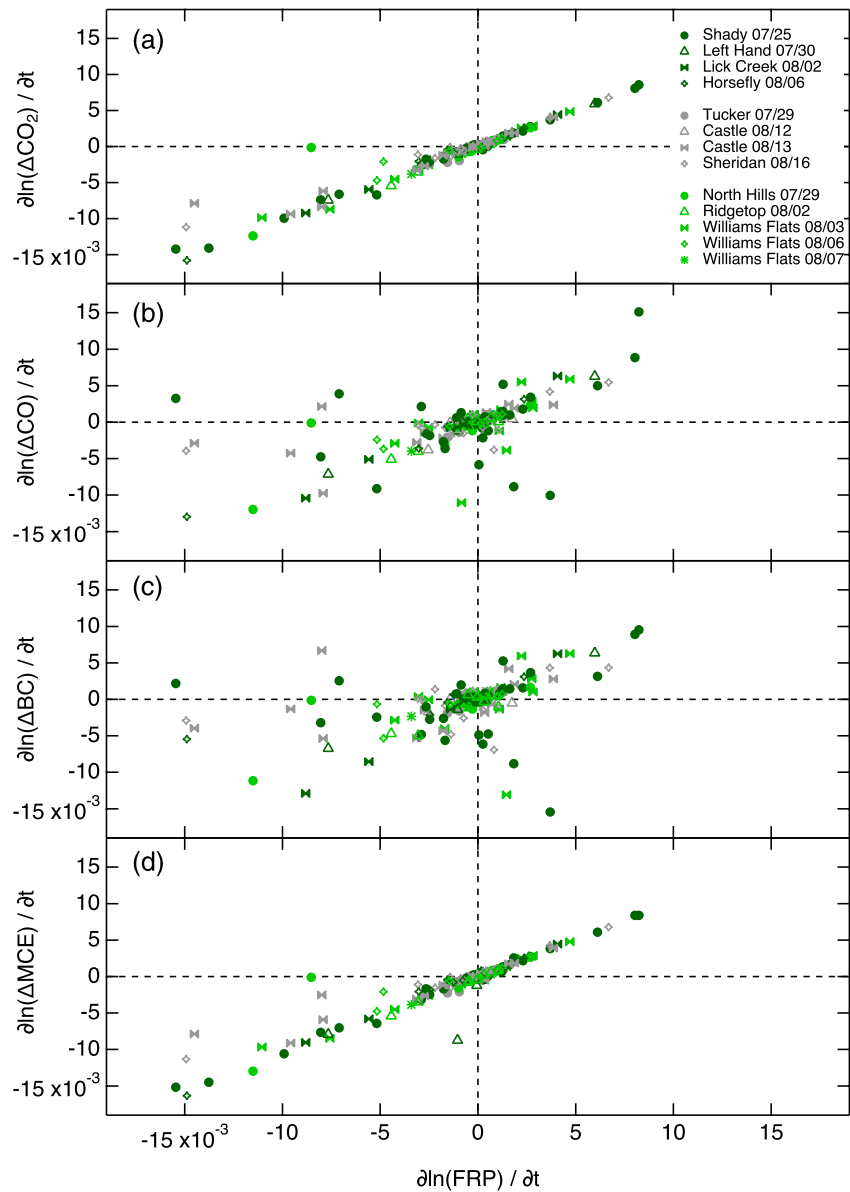


Figure 3. The relative rate of change in CO₂ (a), CO (b), BC (c), and MCE (d) versus the time aligned relative rate of change in GOES FRP. Colors are used to distinguish landcover types with light green representing a mixture of grass/shrubland and forest/woodland, dark green forests/woodlands, and grey grass/shrubland. Dotted black lines show zero change for the x and y axis as a reference.

relationship between fire-integrated FRP and the combustion rate of biomass is well established in the literature and is the basis for top-down fire emissions inventories (Freeborn et al., 2008; Ichoku et al., 2008; Wooster et al., 2003). Figure 3 shows the relationships between the relative rate of change in transect-integrated CO₂, CO, BC, and MCE and the corresponding relative rate of change in integrated FRP observations from GOES.

It is clear that the DC-8 was able to sample fire emissions from periods when the fire activity was both waxing ($\partial \ln(\text{FRP}) / \partial t > 0$) and waning ($\partial \ln(\text{FRP}) / \partial t < 0$). While many fires were sampled during periods of increasing fire activity where both increasing FRP and plume dilution serve to reduce concentrations of conserved tracers during downwind flight legs (relative to the earlier legs), some fires (e.g., Shady on 25 July and Sheridan on 16 August) exhibited a decrease in FRP over time. An example of a fire sampled during periods of increasing FRP is given in Figure 2 for Williams Flats fire, and a counterexample of a fire sampled during

Table 1
Correlations Between the Relative Rate of Change in In Situ Measurements and GOES FRP

Fire	Grass/shrubland						Forest/woodland						Mixed			
	Tucker	Castle		Sheridan	Shady	Left Hand	Lick Creek	Horsefly	North Hills	Ridgetop	High		Williams Flats	Extreme		
Fire danger	Very high	Moderate	High	High	High	Moderate	High	High	High	High	High	High	High	High	High	
Date Sampled	07/29	08/12	08/13	08/16	07/25	07/30	08/02	08/06	07/29	08/02	08/02	08/03	08/06	08/07	08/07	
# Transects	10	15	23	18	43	12	6	10	13	9	9	32	7	21	21	
# Detections	914	180	29	460	367	142	184	181	123	617	617	1,162	1,294	2,813	2,813	
Smoke age	136 ± 76	176 ± 126	102 ± 54	165 ± 111	109 ± 56	334 ± 84	74 ± 44	116 ± 50	101 ± 74	150 ± 55	150 ± 55	178 ± 95	85 ± 41	151 ± 62	151 ± 62	
r (CO ₂ :FRP)	0.98	0.95	0.95	0.99	0.99	0.99	0.99	0.99	0.80	0.99	0.99	0.99	0.93	0.98	0.98	
r (CO:FRP)	0.98	0.78	0.62	0.87	0.66	0.99	0.99	0.99	0.80	0.96	0.96	0.51	0.96	0.94	0.94	
r (BC:FRP)	0.97	0.37	0.36	0.60	0.81	0.99	0.99	0.79	0.79	0.88	0.88	0.67	0.72	0.87	0.87	
r (MCE:FRP)	0.98	0.95	0.94	0.99	0.99	0.84	0.99	0.99	0.80	0.99	0.99	0.99	0.93	0.98	0.98	

Note. Fires are grouped into their dominant landcover type determined using final GeoMAC burned area perimeters and FCCS fuel maps. Observed fire danger, date sampled by the DC-8, the total number of transects per fire, the total number of daily GOES detections, and the average and standard deviation of sampled smoke age (min) are shown in the upper two panels. The third panel shows Pearson's correlation coefficient (r) between the relative rate of change in transect integrated measurements $\left(\frac{\partial \ln(\Delta X)}{\partial t}\right)$ and the relative rate of change in FRP $\left(\frac{\partial \ln(\text{FRP})}{\partial t}\right)$ integrated over the same time interval.

decreasing FRP is shown in Figure S2 for the Sheridan fire. The plume peak time series shown in Figures 2 and S2 highlights the importance of the FRP trend as a governing influence on plume evolution. In Figure 2, the decrease in peak areas with increasing downwind distance is characteristic of plume dilution, while the lack of a decrease shown in Figure S2 implies that the plume is not diluting. It is only with the important context provided by the FRP time series that changing fire activity, rather than dilution, be considered as the primary driver of these starkly contrasting plume trends.

We uncover strong linear correlations ($r > 0.8$) between the relative rate of change in FRP and the relative rate of change in both CO_2 and MCE (Table 1). Figure 3 highlights the exceptionally strong correlation between the rate at which FRP changes with time and the resulting relative temporal change in CO_2 mixing ratio observed by the DC-8 downwind (Panel A). The strong correlations between FRP and CO_2 and MCE are likely because fire carbon emissions are composed of 80–90% CO_2 (Andreae & Merlet, 2001). The correlations remain strong ($r > 0.8$) on days with plentiful GOES detections to inform the diurnal cycle of FRP and also on days with scarce GOES detections when the bimodal Gaussian model fit to the average diurnal FRP cycle was relied on heavily. Smoke age did not have a discernible influence on the correlations over the range of FIREX-AQ variability (<6 hr old). The correlation weakens slightly when FRP and CO_2 are both decreasing, which may be due to the coincident influence of dilution on conserved smoke tracer concentrations. However, if dilution were playing a dominant role, we might expect to see a different slope for these fires in Figure 3a as the dilution process changes $\partial \ln(\text{CO}_2)/\partial t$ without changing $\partial \ln(\text{FRP})/\partial t$. Unraveling the fingerprints of FRP changes versus dilution on plume concentrations may best be done using plume-scale models that are able to resolve both of these processes or by looking at the local turbulence observations from the aircraft that may be related to dilution mixing processes.

The correlation with the relative rate of change in FRP weakens slightly for CO and BC compared to CO_2 . This may reflect the confounding influences of the fire properties on the emission of these incomplete combustion products (although not so much explained by the relative rate of change in MCE). While BC aerosols are also subject to plume processes such as coagulation that reduce their number concentration beyond what would be attributable to dilution with background air alone, the mass concentrations reported here should be largely conserved over the early hours of the plume. Limitations of this analysis include the lack of in situ measurements that span the vertical length of the plume and the potential of horizontal heterogeneity in the distribution of emissions in the plume. Light Detection And Ranging (LIDAR)-derived measurements of vertical bulk aerosol extinction could offer an opportunity to explore the vertical distribution of emissions and the role of boundary layer dynamics on plume extent.

4. Summary and Conclusions

We present a new method for linking changes in conserved emissions tracers to changes in the high time-resolution satellite observations of FRP. The technique is used to interpret the comprehensive airborne data set from the NASA FIREX-AQ mission in summer, 2019. These unique data demonstrate the need for and the power of satellite observations for disentangling the impacts of dilution, atmospheric processing, and changing fire activity on fire emissions observed in smoke plumes. Our results suggest smoke forecast and fire emissions models could leverage assimilation of high time-resolution GOES FRP observations to significantly improve their ability to temporally distribute emissions. The strong relationships between the relative rate of change in FRP and CO_2 ($r > 0.9$) can also be exploited in smoke forecasting and emissions models, as it provides a connection to other trace gas and aerosol emissions. While fire emissions are commonly modeled as a single, Gaussian mode, we show that this representation is oversimplified and would fail to capture the multi-peak structure of the diverse FIREX-AQ fires. The results from this study also imply that high time-resolution GOES FRP observations can be used as a tool to tease apart the influence of changing fire behavior from downwind plume processing when interpreting airborne campaign measurements. The variation in FRP over the time period represented by smoke plumes is an important factor in understanding smoke evolution along the length of a plume and should be considered along with dilution and atmospheric processing. We demonstrate the strong connection between FRP and CO_2 , which suggests that changes in fire activity govern the near-field plume concentrations more so than dilution. Combining airborne measurements with satellite FRP is a powerful analysis tool for accounting for the influence of changing fire activity on plume observations and their downwind evolution.

Data Availability Statement

All data are publicly available from the NASA FIREX-AQ data archive (<https://doi.org/10.5067/suborbital/firexaq2019/data001>).

Acknowledgments

This work was supported by the NASA Tropospheric Chemistry Program managed by Dr. Barry Lefer. E. B. W. is supported by a NASA Postdoctoral Program Fellowship. J. M. K. and J. P. S. are supported by NOAA. We thank the FIREX-AQ project scientists Jim Crawford, Carsten Warneke, and Jack Dibb, as well as the pilots and crew of the NASA DC-8.

References

- Abatzoglou, J. T., & Williams, A. P. (2016). Impact of anthropogenic climate change on wildfire across western US forests. *Proceedings of the National Academy of Sciences of the United States of America*, *113*, 11,770–11,775. <https://doi.org/10.1073/pnas.1607171113>
- Ahmadov, R., Grell, G., James, E., Csiszar, I., Tsidulko, M., & Pierce, B. (2017). International Geoscience and Remote Sensing Symposium (IGARSS). In Institute of Electrical and Electronics Engineers Inc. (Eds.), *Using VIIRS fire radiative power data to simulate biomass burning emissions, plume rise and smoke transport in a real-time air quality modeling system* (Vol. 2017-July, pp. 2806–2808). Fort Worth, TX. <https://doi.org/10.1109/IGARSS.2017.8127581>
- Albini, F. A., & Reinhardt, E. D. (1995). Modeling ignition and burning rate of large woody natural fuels. *International Journal of Wildland Fire*, *5*(2), 81–91. <https://doi.org/10.1071/WF9950081>
- Andela, N., Kaiser, J. W., van der Werf, G. R., & Wooster, M. J. (2015). New fire diurnal cycle characterizations to improve fire radiative energy assessments made from MODIS observations. *Atmospheric Chemistry and Physics*, *15*, 8831–8846. <https://doi.org/10.5194/acp-15-8831-2015>
- Andreae, M. O., & Merlet, P. (2001). Emission of trace gases and aerosols from biomass burning. *Global Biogeochemical Cycles*, *15*(4), 955–966. <https://doi.org/10.1029/2000GB001382>
- Balch, J. K., Bradley, B. A., D'Antonio, C. M., & Gómez-Dans, J. (2013). Introduced annual grass increases regional fire activity across the arid western USA (1980–2009). *Global Change Biology*, *19*, 173–183. <https://doi.org/10.1111/gcb.12046>
- Bond, T. C., Doherty, S. J., Fahey, D. W., Forster, P. M., Berntsen, T., & Deangelo, B. J. (2013). Bounding the role of black carbon in the climate system: A scientific assessment. *Journal of Geophysical Research: Atmospheres*, *118*, 5380–5552. <https://doi.org/10.1002/jgrd.50171>
- Bradshaw, L. S., Deeming, J. E., Burgan, R. E., & Cohen, J. D. (1983). *The 1978 National Fire-Danger Rating System: Technical documentation, USDA Forest Service General Technical Report INT* (Vol. 169). Missoula, MT: United States Department of Agriculture, Forest Service, Intermountain Forest and Range Experiment Station. Retrieved from https://www.fs.fed.us/rm/pubs_int/int_gtr169.pdf
- Freeborn, P. H., Wooster, M. J., Hao, W. M., Ryan, C. A., Nordgren, B. L., Baker, S. P., & Ichoku, C. (2008). Relationships between energy release, fuel mass loss, and trace gas an aerosol emissions during laboratory biomass fires. *Journal of Geophysical Research*, *113*, D01301. <https://doi.org/10.1029/2007JD008679>
- Giglio, L. (2007). Characterization of the tropical diurnal fire cycle using VIIRS and MODIS observations. *Remote Sensing of Environment*, *108*(4), 407–421. <https://doi.org/10.1016/j.rse.2006.11.018>
- Giglio, L., Kendall, J. D., & Justice, C. O. (1999). Evaluation of global fire detection algorithms using simulated AVHRR infrared data. *International Journal of Remote Sensing*, *20*(10), 1947–1985. <https://doi.org/10.1080/014311699212290>
- Goldammer, J. G., Statheropoulos, M., & Andreae, M. O. (2008). Chapter 1 impacts of vegetation fire emissions on the environment, human health, and security: A global perspective. In A. Bytnerowicz, M. J. Arbaugh, A. R. Riebau, & C. Andersen (Eds.), *Developments in environmental science, Wildland Fires and Air Pollution* (Vol. 8, pp. 3–36). Amsterdam, The Netherlands: Elsevier. [https://doi.org/10.1016/S1474-8177\(08\)00001-6](https://doi.org/10.1016/S1474-8177(08)00001-6)
- Hammer, R. B., Stewart, S. I., & Radeloff, V. C. (2009). Demographic trends, the wildland-urban interface, and wildfire management. *Society and Natural Resources*, *22*(8), 777–782. <https://doi.org/10.1080/08941920802714042>
- Hyde, J. C., Smith, A. M. S., Ottmar, R. D., Alvarado, E. C., & Morgan, P. (2011). The combustion of sound and rotten coarse woody debris: A review. *International Journal of Wildland Fire*, *20*, 163. <https://doi.org/10.1071/WF09113>
- Ichoku, C., & Ellison, L. (2014). Global top-down smoke-aerosol emissions estimation using satellite fire radiative power measurements. *Atmospheric Chemistry and Physics*, *14*, 6643–6667. <https://doi.org/10.5194/acp-14-6643-2014>
- Ichoku, C., Giglio, L., Wooster, M. J., & Remer, L. A. (2008). Global characterization of biomass-burning patterns using satellite measurements of fire radiative energy. *Remote Sensing of Environment*, *112*(6), 2950–2962. <https://doi.org/10.1016/j.rse.2008.02.009>
- Jaffe, D., Hafner, W., Chand, D., Westerling, A., & Spracklen, D. (2008). Interannual variations in PM_{2.5} due to wildfires in the Western United States. *Environmental Science and Technology*, *42*(8), 2812–2818. <https://doi.org/10.1021/es702755v>
- Kaiser, J. W., Flemming, J., Schultz, M. G., Suttie, M., & Wooster, M. J. (2009). The MACC Global Fire Assimilation System: First emission products (GFASv0). Retrieved from <http://www.ecmwf.int/publications/>
- Kaiser, J. W., Heil, A., Andreae, M. O., Benedetti, A., Chubarova, N., & Jones, L. (2012). Biomass burning emissions estimated with a global fire assimilation system based on observed fire radiative power. *Biogeosciences*, *9*(1), 527–554. <https://doi.org/10.5194/bg-9-527-2012>
- Kasischke, E. S., & Penner, J. E. (2004). Improving global estimates of atmospheric emissions from biomass burning. *Journal of Geophysical Research*, *109*, D14S01. <https://doi.org/10.1029/2004JD004972>
- Kerns, B. K., Tortorelli, C., Day, M. A., Nietupski, T., Barros, A. M. G., Kim, J. B., & Krawchuk, M. A. (2020). Invasive grasses: A new perfect storm for forested ecosystems? *Forest Ecology and Management*, *463*, 117985. <https://doi.org/10.1016/j.foreco.2020.117985>
- Kochi, I., Donovan, B., H. G., Champ, P. A., & Loomis, J. B. (2010). The economic cost of adverse health effects from wildfire-smoke exposure: A review. *International Journal of Wildland Fire*, *19*(7), 803–817. <https://doi.org/10.1071/WF09077>
- Langmann, B., Duncan, B., Textor, C., Trentmann, J., & van der Werf, G. R. (2009). Vegetation fire emissions and their impact on air pollution and climate. *Atmospheric Environment*, *43*(1), 107–116. <https://doi.org/10.1016/j.atmosenv.2008.09.047>
- Larkin, N. K., Raffuse, S. M., & Strand, T. M. (2014). Wildland fire emissions, carbon, and climate: U.S. emissions inventories. *Forest Ecology and Management*, *317*, 61–69. <https://doi.org/10.1016/j.foreco.2013.09.012>
- Li, F., Val Martin, M., Andreae, M. O., Arneeth, A., Hantson, S., & Kaiser, J. W. (2019). Historical (1700–2012) global multi-model estimates of the fire emissions from the Fire Modeling Intercomparison Project (FireMIP). *Atmospheric Chemistry and Physics*, *19*, 12,545–12,567. <https://doi.org/10.5194/acp-19-12545-2019>
- Li, F., Zhang, X., Kondragunta, S., & Csiszar, I. (2018). Comparison of fire radiative power estimates from VIIRS and MODIS observations. *Journal of Geophysical Research: Atmospheres*, *123*, 4545–4563. <https://doi.org/10.1029/2017JD027823>
- Li, F., Zhang, X., Kondragunta, S., Schmidt, C. C., & Holmes, C. D. (2020). A preliminary evaluation of GOES-16 active fire product using Landsat-8 and VIIRS active fire data, and ground-based prescribed fire records. *Remote Sensing of Environment*, *237*, 111600. <https://doi.org/10.1016/j.rse.2019.111600>

- Li, F., Zhang, X., Roy, D. P., & Kondragunta, S. (2019). Estimation of biomass-burning emissions by fusing the fire radiative power retrievals from polar-orbiting and geostationary satellites across the conterminous United States. *Atmospheric Environment*, *211*, 274–287. <https://doi.org/10.1016/j.atmosenv.2019.05.017>
- Liu, J. C., Pereira, G., Uhl, S. A., Bravo, M. A., & Bell, M. L. (2015). A systematic review of the physical health impacts from non-occupational exposure to wildfire smoke. *Environmental Research*, *136*, 120–132. <https://doi.org/10.1016/j.envres.2014.10.015>
- Liu, T., Mickley, L. J., Marlier, M. E., DeFries, R. S., Khan, M. F., Latif, M. T., & Karambelas, A. (2020). Diagnosing spatial biases and uncertainties in global fire emissions inventories: Indonesia as regional case study. *Remote Sensing of Environment*, *237*, 111557. <https://doi.org/10.1016/j.rse.2019.111557>
- Loehman, R. A., Reinhardt, E., & Riley, K. L. (2014). Wildland fire emissions, carbon, and climate: Seeing the forest and the trees—A cross-scale assessment of wildfire and carbon dynamics in fire-prone, forested ecosystems. *Forest Ecology and Management*, *317*, 9–19. <https://doi.org/10.1016/j.foreco.2013.04.014>
- Lu, X., Zhang, L., Yue, X., Zhang, J., Jaffe, D. A., & Stohl, A. (2016). Wildfire influences on the variability and trend of summer surface ozone in the mountainous western United States. *Atmospheric Chemistry and Physics*, *16*, 14,687–14,702. <https://doi.org/10.5194/acp-16-14687-2016>
- Mell, W. E., Manzello, S. L., Maranghides, A., Butry, D., & Rehm, R. G. (2010). The wildland–urban interface fire problem—Current approaches and research needs. *International Journal of Wildland Fire*, *19*, 238. <https://doi.org/10.1071/WF07131>
- Menakis, J. P., Osborne, D., & Melanie, M. (2003). Fire, fuel treatments and ecological restoration: Conference proceedings. In USDA Forest Service Proceedings (pp. 281–287).
- Mota, B., & Wooster, M. J. (2018). A new top-down approach for directly estimating biomass burning emissions and fuel consumption rates and totals from geostationary satellite fire radiative power (FRP). *Remote Sensing of Environment*, *206*, 45–62. <https://doi.org/10.1016/j.rse.2017.12.016>
- Mu, M., Randerson, J. T., Van Der Werf, G. R., Giglio, L., Kasibhatla, P., & Morton, D. (2011). Daily and 3-hourly variability in global fire emissions and consequences for atmospheric model predictions of carbon monoxide. *Journal of Geophysical Research*, *116*, D24303. <https://doi.org/10.1029/2011JD016245>
- Ottmar, R. D., Sandberg, D. V., Riccardi, C. L., & Prichard, S. J. (2007). An overview of the Fuel Characteristic Classification System—Quantifying, classifying, and creating fuelbeds for resource planning. Special Forum on the Fuel Characteristic Classification System. *Canadian Journal of Forest Research*, *37*(12), 2383–2393. <https://doi.org/10.1139/X07-077>
- Pack, D. W., Rice, C. J., Tressel, B. J., Lee-Wagner, C. J., & Oshika, E. M. (2000). Civilian uses of surveillance satellites. *Crosslink*, *1*(1), 2–8.
- Pan, X., Ichoku, C., Chin, M., Bian, H., Darmenov, A., & Colarco, P. (2020). Six global biomass burning emission datasets: Intercomparison and application in one global aerosol model. *Atmospheric Chemistry and Physics*, *20*(2), 969–994. <https://doi.org/10.5194/acp-20-969-2020>
- Pierce, R. B., Schaack, T., al-Saadi, J. A., Fairlie, T. D., Kittaka, C., Lingenfeller, G., et al. (2007). Chemical data assimilation estimates of continental U.S. ozone and nitrogen budgets during the Intercontinental Chemical Transport Experiment–North America. *Journal of Geophysical Research*, *112*, D12S21. <https://doi.org/10.1029/2006JD007722>
- Reid, C. E., Brauer, M., Johnston, F. H., Jerrett, M., Balmes, J. R., & Elliott, C. T. (2016). Critical review of health impacts of wildfire smoke exposure. *Environmental Health Perspectives*, *124*, 1334–1343. <https://doi.org/10.1289/ehp.1409277>
- Roberts, G., Wooster, M. J., & Lagoudakis, E. (2009). Annual and diurnal african biomass burning temporal dynamics. *Biogeosciences*, *6*(5), 849–866. <https://doi.org/10.5194/bg-6-849-2009>
- Sachse, G. W., Collins, J. E. Jr., Hill, G. F., Wade, L. O., Burney, L. G., & Ritter, J. A. (1991). Airborne tunable diode laser sensor for high-precision concentration and flux measurements of carbon monoxide and methane. *Measurement of Atmospheric Gases*, *1433*, 157–166. <https://doi.org/10.1117/12.46162>
- Saide, P. E., Peterson, D. A., da Silva, A., Anderson, B., Ziemba, L. D., & Diskin, G. (2015). Revealing important nocturnal and day-to-day variations in fire smoke emissions through a multiplatform inversion. *Geophysical Research Letters*, *42*, 3609–3618. <https://doi.org/10.1002/2015GL063737>
- Schmidt, C. (2019). Monitoring fires with the GOES-R series. In *The GOES-R series: A new generation of geostationary environmental satellites* (pp. 145–163). Amsterdam, The Netherlands: Elsevier. <https://doi.org/10.1016/B978-0-12-814327-8.00013-5>
- Schroeder, M. J. (1970). *Fire weather: A guide for application of meteorological information to forest fire control operations, agriculture handbook*, 360. Washington, DC: US Department of Agriculture, Forest Service.
- Shi, Y., Matsunaga, T., Saito, M., Yamaguchi, Y., & Chen, X. (2015). Comparison of global inventories of CO₂ emissions from biomass burning during 2002–2011 derived from multiple satellite products. *Environmental Pollution*, *206*, 479–487. <https://doi.org/10.1016/j.envpol.2015.08.009>
- Sommers, W. T., Loehman, R. A., & Hardy, C. C. (2014). Wildland fire emissions, carbon, and climate: Science overview and knowledge needs. *Forest Ecology and Management*, *317*, 1–8. <https://doi.org/10.1016/j.foreco.2013.12.014>
- Stavros, E. N., Abatzoglou, J., Larkin, N. K., McKenzie, D., & Steel, E. A. (2014). Climate and very large wildland fires in the contiguous western USA. *International Journal of Wildland Fire*, *23*, 899. <https://doi.org/10.1071/WF13169>
- Theobald, D. M., & Romme, W. H. (2007). Expansion of the US wildland-urban interface. *Landscape and Urban Planning*, *83*(4), 340–354. <https://doi.org/10.1016/j.landurbplan.2007.06.002>
- Thonicke, K., Spessa, A., Prentice, I. C., Harrison, S. P., Dong, L., & Carmona-Moreno, C. (2010). The influence of vegetation, fire spread and fire behaviour on biomass burning and trace gas emissions: Results from a process-based model. *Biogeosciences*, *7*(6), 1991–2011. <https://doi.org/10.5194/bg-7-1991-2010>
- Urbanski, S. (2014). Wildland fire emissions, carbon, and climate: Emission factors. *Forest Ecology and Management*, *317*, 51–60. <https://doi.org/10.1016/j.foreco.2013.05.045>
- van der Werf, G. R., Randerson, J. T., Giglio, L., van Leeuwen, T. T., Chen, Y., & Rogers, B. M. (2017). Global fire emissions estimates during 1997–2016. *Earth System Science Data*, *9*(2), 697–720. <https://doi.org/10.5194/essd-9-697-2017>
- Vay, S. A., Woo, J. H., Anderson, B. E., Thornhill, K. L., Blake, D. R., Westberg, D. J., et al. (2003). Influence of regional-scale anthropogenic emissions on CO₂ distributions over the western North Pacific. *Journal of Geophysical Research*, *108*(D20), 8801. <https://doi.org/10.1029/2002JD003094>
- Walters, S. P., Schneider, N. J., & Guthrie, J. D. (2011). Geospatial Multi-Agency Coordination (GeoMAC) wildland fire perimeters, 2008. U.S. Geological Survey Data Series, 612, 6.
- Ward, D. E., & Radke, L. F. (1993). Emissions measurements from vegetation fires: A comparative evaluation of methods and results. In P. J. Crutzen, J. G. Goldammer (Eds.), *Fire in the environment: The ecological, atmospheric, and climatic importance of vegetation fires* (Dahlem Workshop, pp. 53–76). Chichester, England: John Wiley & Sons.

- Westerling, A. L., Hidalgo, H. G., Cayan, D. R., & Swetnam, T. W. (2006). Warming and earlier spring increase Western U.S. forest wildfire activity. *Science*, *313*(5789), 940–943. <https://doi.org/10.1126/science.1128834>
- Wiedinmyer, C., Akagi, S. K., Yokelson, R. J., Emmons, L. K., Al-Saadi, J. A., Orlando, J. J., & Soja, A. J. (2011). The Fire INventory from NCAR (FINN): A high resolution global model to estimate the emissions from open burning. *Geoscientific Model Development*, *4*(3), 625–641. <https://doi.org/10.5194/gmd-4-625-2011>
- Wiggins, E. B., Veraverbeke, S., Henderson, J. M., Karion, A., Miller, J. B., Lindaas, J., et al. (2016). The influence of daily meteorology on boreal fire emissions and regional trace gas variability. *Journal of Geophysical Research: Biogeosciences*, *121*, 2793–2810. <https://doi.org/10.1002/2016JG003434>
- Wooster, M. J., Zhukov, B., & Oertel, D. (2003). Fire radiative energy for quantitative study of biomass burning: Derivation from the BIRD experimental satellite and comparison to MODIS fire products. *Remote Sensing of Environment*, *86*(1), 83–107. [https://doi.org/10.1016/S0034-4257\(03\)00070-1](https://doi.org/10.1016/S0034-4257(03)00070-1)
- Xie, Y., Lin, M., & Horowitz, L. W. (2020). Summer PM_{2.5} pollution extremes caused by wildfires over the western United States during 2017–2018. *Geophysical Research Letters*, *47*, e2020GL089429. <https://doi.org/10.1029/2020GL089429>
- Yokelson, R. J., Karl, T., Artaxo, P., Blake, D. R., Christian, T. J., Griffith, D. W., et al. (2007). The tropical forest and fire emissions experiment: Overview and airborne fire emission factor measurements. *Atmospheric Chemistry and Physics*, *7*(19), 5175–5196. <https://doi.org/10.5194/acp-7-5175-2007>
- Zhang, X., & Kondragunta, S. (2008). Temporal and spatial variability in biomass burned areas across the USA derived from the GOES fire product. *Remote Sensing of Environment*, *112*(6), 2886–2897. <https://doi.org/10.1016/j.rse.2008.02.006>
- Zhang, X., Kondragunta, S., Ram, J., Schmidt, C., & Huang, H. C. (2012). Near-real-time global biomass burning emissions product from geostationary satellite constellation. *Journal of Geophysical Research*, *117*, D14201. <https://doi.org/10.1029/2012JD017459>